

Sigma meson in pole-dominated QCD sum rules

Toru Kojo¹ and Daisuke Jido²

¹*Department of Physics, Kyoto University, Kyoto 606-8502, Japan*

²*Yukawa Institute for Theoretical Physics, Kyoto University, Kyoto 606-8502, Japan*

(Dated: October 31, 2018)

The properties of $\sigma(600)$ meson are studied using the QCD sum rules (QSR) for the tetraquark operators. In the SU(3) chiral limit, we investigate separately SU(3) singlet and octet tetraquark states as constituents of the σ meson, and discuss their roles for the classification of the light scalar nonets, σ, f_0, a_0 , and κ , as candidates of tetraquark states. All our analyses are performed in the suitable Borel window which is indispensable to avoid the *pseudo peak* artifacts outside of the Borel window. The acceptably wide Borel window originates after preparing the favorable set up of a linear combination of operators and the inclusion of the dimension 12 terms in the OPE. Taking into account for the possible large width, we estimate masses for singlet and octet states as $700 \sim 850$ MeV, $600 \sim 750$ MeV, respectively, although octet states have smaller overlap with the pole than singlet state and may be strongly affected by low energy scattering states. This splitting of singlet and octet states emerges from the number of the $\bar{q}q$ annihilation diagrams, which include both color singlet annihilation processes, $qq\bar{q}\bar{q} \rightarrow (q\bar{q})_1$ and color octet annihilation processes, $qq\bar{q}\bar{q} \rightarrow G(q\bar{q})_8$. The mass evaluation for the σ meson gives the value around $600 \sim 800$ MeV which is much smaller than the mass obtained by 2-quark correlators, $1.0 \sim 1.2$ GeV. This indicates σ state has the large overlap with the tetraquark states.

PACS numbers: 12.39.Mk, 11.55.Hx, 11.30.Rd

I. INTRODUCTION

The structure of scalar mesons is a long-standing problem in hadron spectroscopy [1]. In contrast to the other hadrons, two flavor nonets appear around 1 GeV in the scalar meson spectra. The systematic classification of scalar mesons sheds light on the nonperturbative aspects of QCD. Especially, the lighter scalar nonet, the isoscalar $\sigma(600)$, $f_0(980)$, the isodoublet $\kappa(800)$, and the isovector $a_0(980)$, are candidates for exotic hadrons (exotics) which have more complicated components than simple mesonic $q\bar{q}$ or baryonic qqq structure. The naive $q\bar{q}$ assignment of the constituent quark picture for these mesons, $\sigma \sim (u\bar{u} + d\bar{d})$, $f_0 \sim s\bar{s}$, $\kappa \sim u\bar{s}$, $a_0 \sim (u\bar{u} - d\bar{d})$, may lead the unrealistic mass ordering, $m(\sigma) \sim m(a_0) < m(\kappa) < m(f_0)$, and suggest heavier masses due to the P-wave angular excitation between two quarks, which typically costs 500 MeV, for the $J^P = 0^+$ quantum number of the scalar mesons. It is believed that these $q\bar{q}$ assignments are most likely realized in the nonet above 1 GeV rather than the nonet below 1 GeV.

The masses of the light scalar mesons are explained by several pictures. One of them is the four quark picture proposed by Jaffe [2]. In this picture, assuming the quark contents with the ideal mixing of the flavor as $\sigma \sim (ud)(\bar{u}\bar{d})$, $f_0 \sim [(ds)(\bar{d}\bar{s}) + (su)(\bar{s}\bar{u})]$, $\kappa \sim (ud)(\bar{s}\bar{u})$, $a_0 \sim [(ds)(\bar{d}\bar{s}) - (su)(\bar{s}\bar{u})]$, one can naturally explain the observed mass ordering. For σ meson, quenched lattice calculations also support this assignment [3, 4]. Qualitatively, one of the key ideas for the considerable mass reduction of the light scalar mesons below 1 GeV is to employ the possible strong diquark correlation originated from the chromo-magnetic interaction [2]. This brings us to an interesting possibility that the scalar mesons are

considered as the good place to investigate the strength of diquark correlation, which may provide a useful building block to understand the hadron spectra [5] and for the further applications to the hot/dense quark matter [6].

Mixing of the two and four quark components is also employed to explain the scalar meson spectra. For example, the scalar nonet above 1 GeV have larger mass than one expected from the $q\bar{q}$ picture in the conventional quark models, as seen in the anomalous spin-orbit splitting, $a_1(1230) < a_2(1320) < a_0(1450)$, in contrast to the charmonium mass splitting $\chi_{c0}(3414) < \chi_{c1}(3510) < \chi_{c2}(3556)$. This mass ordering could be explained by a mixing scenario of the two and four quark components, in which, as a result of the level repulsion, the mass of the four-quark dominated state gets reduced, while the two-quark dominated state is pushed up [7].

For the isoscalar sector, σ and f_0 , Narison discussed another possibility [8] invoking the QCD sum rule (QSR) [9, 10] and some low energy theorems [11]. In his scenario, the glueball degrees of freedom come into play and the strong $q\bar{q} - G^2$ mixing leads the considerable mass reduction below 1 GeV although unmixed glueball and $q\bar{q}$ are expected to be relatively heavy, ~ 1.6 GeV [12] and ~ 1.4 GeV [4], respectively, in the quenched lattice calculations. The strength of the $q\bar{q} - G^2$ mixing has been studied in various approaches, but the strong mixing has not been confirmed yet [13].

The hadronic picture for the scalar meson were also widely discussed. The σ , $\kappa(800)$, $f_0(980)$ and $a_0(980)$ are dynamically generated as quasi-bound resonance states in scattering of the Nambu-Goldstone bosons based on chiral dynamics with an appropriate treatment for restoring unitarity in the scattering amplitudes [14].

The σ meson itself is an attractive subject of contem-

porary nuclear physic. The σ field is the origin of the attractive part of the nuclear force in the intermediate energy region [15] and can be a chiral partner of the pion being a possible soft mode in the chiral restoration [16]. Its existence of the σ meson had been a long-standing problem, but recent experimental results such as $D^+ \rightarrow \pi^+\pi^+\pi^-$ [17], $J/\psi \rightarrow \omega\pi^+\pi^-$ [18], and dispersion analysis employing Roy equation [19] support the existence of the σ pole with mass $440 \sim 540$ MeV and width $250 \sim 540$ MeV.

Yet the structure of the scalar mesons is not conclusive. We have several pictures of the constituents of the scalar meson with their admixtures. One of the purposes in this paper is to discuss the relevant constituents and the mixing scheme. They can be investigated through comparison of the several correlators utilizing in the QSR [9, 10], which relates the nonperturbative aspects of QCD to the hadronic properties. In this work, our main consideration is on the four-quark (4q) picture for the light scalar nonet and we employ the tetraquark operators to obtain large overlap with the tetraquark states. We will show that the correlators of the tetraquark operators include not only four-quark connected diagrams but also disconnected diagrams, such as the $(q\bar{q})_1$ and $(q\bar{q})_8G$ in the intermediate states. These mixing effects can be studied from the difference between SU(3) flavor singlet and octet correlators. In fact, the number of the annihilation diagrams is four times larger in the singlet case than in the octet case. In our operator case, this leads larger low energy enhancement in the flavor singlet case. Throughout this paper, to avoid the complication from the current quark mass effects, we take the SU(3) chiral limit, in which the singlet and octet states completely decouple.

For the tetraquark analyses with QSR of the σ meson, we have several technical issues to be solved. The most important point is that the resonance mass should be extracted within so-called *Borel window* in which the QSR works with better accuracy. The Borel mass M is introduced to the QSR by a derivative operation L_M to the dispersion relation of the correlation function Π as

$$L_M \Pi^{ope}(-Q^2) = \int_0^\infty ds e^{-s/M^2} \frac{1}{\pi} \text{Im} \Pi^h(s), \quad (1)$$

where $L_M \equiv d^n/(dQ^2)^n$ taking $n \rightarrow \infty$ and $Q^2 \rightarrow \infty$ being fixed by $Q^2/n = M^2$. The correlation function Π^{ope} in the left hand side is calculated by the operator product expansion (OPE) and Π^h in the right hand side is expressed by hadronic contributions. The tower of successes in reproducing the meson and baryon spectra is attributed to appropriate and careful applications of QSR in suitable Borel mass region, i.e., *Borel window*. Only within the Borel window, one is allowed to extract the low energy properties of the spectral integral.

The main technical problem for the multi-quark QSR is that the setting up the Borel window becomes quite difficult. In contrast to the usual meson and baryon cases [20], since correlation functions of multi-quark interpolating fields show slow convergence of OPE and unwelcome

high energy contamination dominates the spectral integrals. As we will emphasize in Sec.IIA and IIB, this leads difficulties to extract low energy properties of the spectral function and we are often stuck with the *pseudo* peak artifacts outside of the Borel window.

All these issues can be solved by use of suitable interpolating fields and inclusion of the OPE terms up to dimension 12 (dim.12) for the tetraquark operators. After that, the Borel windows are found and we can investigate the physical quantities within the Borel windows. To complete solving these issues, we would like to add one more analysis for the σ meson in QSR with the tetraquark operator despite tetraquark operator analysis for the σ meson, although there have been many works done in the past [21, 22].

Another important aspect when we discuss the σ meson is its possible large width and the effects on the mass evaluation of σ . In Sec.IIC, we discuss the Borel transformed Breit-Wigner type spectral function and test how they behave in the effective mass plot. We find the stability is moderate even up to ~ 400 MeV width. As related to this, we re-examine the usual criteria to fix s_{th} . They are reflected to the estimations for the physical quantities of the σ meson.

The organization of this paper is as follows. In Sec.II, we explain the basic concepts of QSR and illustrate the typical pseudo-peak artifacts which we often encounter. The importance to set the Borel window is emphasized. The effects of the width on the effective mass plot are illustrated, and the criterion to fix s_{th} is re-examined. In Sec.III, we discuss the flavor singlet and octet states in the chiral limit. We also argue that both color singlet and octet annihilation diagrams are source to split the singlet and octet states. This splitting may be important to classify f_0 , κ , a_0 even after taking realistic quark mass, which will be discussed in the subsequent paper. In Sec.IV, we show the results of the Borel analyses for the sigma meson together with the singlet and octet states. At first we introduce the tetraquark operator used in the analyses as a linear combination of two types of diquark-diquark local operators. We discuss the criteria to determine the mixing angle of the operators. After fixing it, we perform the Borel analysis. For the singlet state we obtain the mass value $700 \sim 850$ MeV, while, for octet state, we estimate the mass $600 \sim 750$ MeV, although the residue of the octet state is much smaller than the singlet state and thus may be affected by low energy scattering background. Finally we examine the σ meson as superposition of singlet and octet states and estimate its mass $600 \sim 800$ MeV within error of width effects. The Sec.V and VI are devoted to discussion and summary, respectively. All the details about the OPE terms and operator dependence are summarized in the Appendix.

II. THE BASIC CONCEPTS OF QSR AND POSSIBLE PSEUDO-PEAK ARTIFACTS

In this section, we start with a brief review of the basic concepts of QSR, especially emphasizing the importance of the Borel window. Definitions of the terminologies and notations used in the later analyses are given in Sec.II A. In Sec.II B, we illustrate a typical artifact in the sum rules, *pseudo peak artifact*, which often appears in QSR for the exotic hadrons. We show that imposing correct criteria on the Borel window rejects such an artifact. In Sec.II C, we examine the width effects on the Borel stability plots for the effective mass and residue. The way to determine the threshold parameter s_{th} is also discussed in detail.

A. Basic concepts of QSR

Following the standard way of the QCD sum rule, we start with the time-ordered two-point correlation function of a tetraquark interpolating field J for the scalar meson:

$$\Pi(q^2) \equiv i \int d^4x e^{iq \cdot x} \langle 0 | T [J(x) J^\dagger(0)] | 0 \rangle, \quad (2)$$

where $\langle 0 | \dots | 0 \rangle$ denotes a vacuum expectation value. (Hereafter we write it as $\langle \dots \rangle$ for brevity.) The QSR is then obtained through the dispersion relation,

$$\text{Re}\Pi(q^2) = \text{P} \int_0^\infty ds \frac{1}{\pi} \frac{\text{Im}\Pi(s)}{(s - q^2)} \quad (3)$$

satisfying the the spectral conditions, $\text{Im}\Pi(s) \geq 0$. For sufficiently large $-q^2$, the left hand side of (3) can be expressed by the operator product expansion (OPE) with C_i including the vacuum condensates:

$$\Pi_i^{ope}(q^2) = \sum_{j=0}^4 C_{2j} (q^2)^{4-j} \log(-q^2) + \sum_{j=1}^\infty \frac{C_{8+2j}}{(q^2)^j}. \quad (4)$$

The OPE starts from $(q^2)^4 \log(-q^2)$ reflecting the large number of quark fields in the tetraquark interpolating field. This turns out to be the main origin of QSR artifacts as discussed in Sec.II B.

The imaginary part in the right hand side of Eq.(3) is deemed to be the hadronic spectrum. Based on the quark hadron duality ansatz, we approximate higher energy part of the spectral function than a threshold s_{th} to the spectral function obtained by OPE:

$$\text{Im}\Pi^h(s) = \theta(s_{th} - s) \text{Im}\Pi^h(s) + \theta(s - s_{th}) \text{Im}\Pi^{ope}(s). \quad (5)$$

Here we introduce the threshold parameter s_{th} where the quark hadron duality ansatz begins to work. (We use the notation $E_{th} \equiv \sqrt{s_{th}}$ in the following.) Hereafter, we write the first term of the right hand side of Eq.(5) as

$$\Pi^<(s) \equiv \theta(s_{th} - s) \text{Im}\Pi^h(s) \quad (6)$$

for the later convenience. In usual QSRs, the low energy part $\Pi^<$ is parametrized by a delta function, $\lambda^2 \delta(s - m^2)$ with the pole mass m and the overlap residue λ of the interpolating field J and the hadronic state. Instead, we do not specify the form of $\Pi^<$ at this stage, since we also consider more general contributions from the resonance width and background scattering.

Substituting the expressions Eqs.(4) and (5) into Eq.(3) and using Eq.(1), we obtain the Borel transformed expression of the sum rule

$$\int_0^{s_{th}} ds e^{-s/M^2} \frac{1}{\pi} \text{Im}\Pi^<(s) = \sum_{j=1}^\infty \frac{(-)^j}{\Gamma(j)} \frac{C_{8+2j}}{(M^2)^{j-1}} + \left(\int_0^\infty - \int_{s_{th}}^\infty \right) ds e^{-s/M^2} \sum_{j=0}^4 C_{2j} s^{4-j}, \quad (7)$$

with the Gamma function $\Gamma(n) = (n - 1)!$. Calculating the Wilson coefficients in the right side, we can evaluate the hadronic parameters in the left side as outputs. Here the Borel transformation improves the OPE convergence by factor $1/\Gamma(j)$. At the same time, this transformation reduces the contaminations from high energy states due to the exponential factor e^{-s/M^2} .

Using the equality (7), the *effective* mass and residue are derived as

$$m_{\text{eff}}^2(M^2) \equiv \frac{\int_0^{s_{th}} ds e^{-s/M^2} s \text{Im}\Pi^<(s)}{\int_0^{s_{th}} ds e^{-s/M^2} \text{Im}\Pi^<(s)}, \quad (8)$$

$$\lambda_{\text{eff}}^2(M^2) \equiv e^{m_{\text{eff}}^2(M^2)/M^2} \times \int_0^{s_{th}} ds e^{-s/M^2} \text{Im}\Pi^<(s), \quad (9)$$

in the similar way to mass evaluation in lattice calculations. The reason that we call these values as “effective” mass and residue is that m_{eff} and λ_{eff} include not only pole mass contribution but also the effects of the width and the background. In the usual one peak ansatz, the width and background effects are regarded as small, and then the physical variables should behave independently on the Borel mass and s_{th} is chosen to satisfy this criterion. (More detailed discussion for how to fix s_{th} is given in Sec.II C.)

Now we turn to the explanation for the situation where QSR is workable. In any estimation of the physical quantities, it is required that Eq.(7) holds with good accuracy. This is satisfied after the suitable selection of the Borel mass which achieves the good OPE convergence and reduces the unwanted contaminations from high energy states. Such a region for the Borel mass is called Borel window. This is important both conceptually and practically to derive definite results. A conceptual importance is already emphasized just above. Practically, the Borel window is useful to reject the artifacts. An explicit example will be shown in Sec.II B.

The Borel window in our analysis is determined as follows based on Ref. [10]: The lower boundary of the window is set up so as to make the OPE convergence sufficient in higher-dimensional operators. The criterion is

quantified so that the highest-dimensional terms in the truncated OPE are less than 10% of its whole OPE, i.e.,

$$A(M^2) \equiv \left| \frac{\text{dim.}n \text{ terms}}{\text{OPE summed up to dim.}n} \right| \leq 0.1. \quad (10)$$

At the same time, the higher boundary of the window is fixed by the pole-dominance condition that

$$B(M^2; s_{th}) \equiv \frac{\int_0^{s_{th}} ds e^{-s/M^2} \text{Im}\Pi^<(s)}{\int_0^\infty ds e^{-s/M^2} \text{Im}\Pi(s)} \geq 0.5. \quad (11)$$

Setting up the Borel window is the most important step for the application of the sum rules to discuss the low energy side in the spectral integral, especially for exotic hadrons, as emphasized in [20]. However, this important step was sometimes neglected in the literature for the exotics. Therefore their successes seem to be partial. Outside of the Borel window, we are stuck with the sum rules artifacts, i.e., the artificial stability of the physical quantities against the variation of the Borel mass. Further, the evaluation of the physical properties, mass, residue and so on, depends on the selection of s_{th} so strongly that QSR loses the predictive power. In the next subsection, we will illustrate the origin of the artifacts using some examples.

B. Pseudo peak artifacts

In the following arguments, we consider one of the simplest spectral functions having only the dim.0 term proportional to s^4 in the tetraquark operator case. This case study provides a good example to examine typical artifacts in the QSR for the exotics. Similarly this is the case if we consider only the lower dimension terms proportional to s^n ($n > 0$), and then we recognize the importance of the higher dimension terms dim.8, 10, 12,... beyond the polynomials in OPE.

Equation (7) with only dim.0 term becomes

$$\int_0^{s_{th}} ds e^{-s/M^2} \frac{1}{\pi} \text{Im}\Pi^<(s) = \int_0^{s_{th}} ds e^{-s/M^2} C_0 s^4, \quad (12)$$

where the value of the coefficient C_0 is irrelevant in the following discussion. We expect that the dim.0 term poorly contains the low energy correlation, because the polynomial s^4 drastically decreases in small s region, while s^4 increases rapidly with larger s . Then if we use such a simply increasing function as the spectral function for the sum rules, we encounter unphysical Borel stability for the mass and residue, since the function cut above E_{th} behaves like a peak function as seen in the upper left panel in Fig.1. We call this *pseudo peak* artifact which often appears in the QSR without including enough higher dimension terms beyond the simple polynomial s^n ($n > 0$).

Let us see how *pseudo peak* artifact affects the QCD sum rules. As seen in the lower panels of Fig.1, both

effective mass and residue plots show the stability in the larger M^2 region, as a result that the spectral function just below E_{th} behaves like a peak without large suppression from the factor e^{-s/M^2} . It is important point that they exhibit the strong sensitivity to the threshold parameter. This is a consequence that the E_{th} value directly determines the position of the *pseudo peak*. For the effective mass illustrated in lower left panel of Fig.1, the change of E_{th} by 200 MeV leads the mass change of typically 150 MeV. The strong change is unphysical because E_{th} , in principle, does not have any direct relations with the position of the resonance peak. The threshold dependence is more clearly seen in the effective residue plot. Since the spectrum increases like s^4 , taking larger E_{th} leads the drastic increase of the *pseudo peak* strength, as illustrated in lower right panel of Fig.1.

This artifact can be easily found out by the examination of the rate of the pole dominance even when we treat more complicated spectral functions than that we use now. Shown in the upper right panel of Fig.1 is the pole dominance ratio $B(M^2; s_{th})$ defined in Eq.(11) as the function of M^2 , which is typical quantity to measure the strength of the low energy correlation compared to the unwanted high energy correlation. The exponential factor in Eq.(12) enables to extract the low energy part of the spectral function. The ratio $B(M^2; s_{th})$ determines the upper bound of the applicable range of the sum rule in terms of the Borel mass (Borel window). As seen in two lower panels of Fig.1, the artificial stability is seen above the upper bound of the Borel window, which is indicated by arrow in the figure. In this way, the condition of the sufficient pole dominance rejects the results with artificial stabilities. This is one of the practical usages of the Borel window.

Throughout this section, we have seen the origin of the QSR artifact outside of the Borel window. The lessons we can learn from these examples are the terms with higher dimension like dim.8 have crucial importance to include low energy correlation and to be free from artifacts. In connection with the criterion on the Borel window, the inclusion of higher dimension terms improves the pole dominance and considerably extend the upper bound of the Borel window. In addition to the ensurance of the OPE convergence, this is another reason that we include the higher dimension terms up to dim.12.

C. Possible width effects on the plot of the physical quantities and examination for the threshold fixing criterion

Most of the light scalar nonets are considered to have large widths typically 100 ~ 400 MeV though they have not been well-determined yet. It is important to check how their widths affect the effective mass and residue plots. In this section, we employ as a test function a simplest spectral function including the width, i.e., Breit-

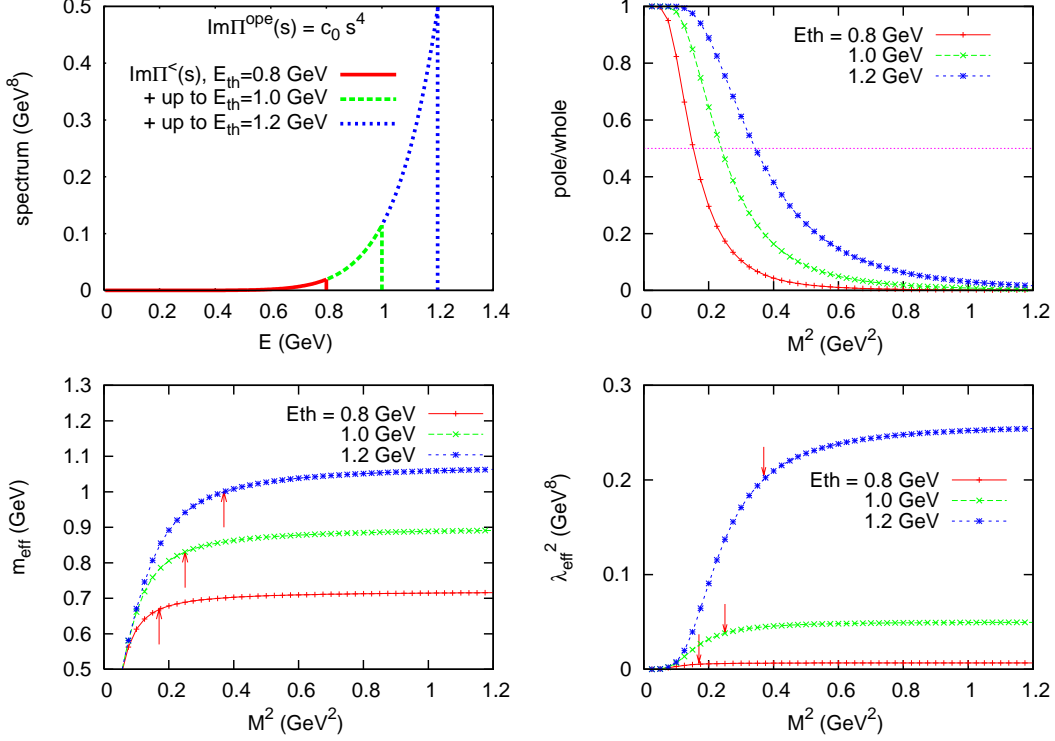


FIG. 1: (Color online) The examples of the pseudo peak artifacts. The upper left panel is the plot of the spectral function with the dim.0 term of the OPE up to the thresholds, $E_{th} = 0.8, 1.0$ and 1.2 GeV. The rapid enhancement of the polynomial s^4 mimics the peak just below $s_{th} = E_{th}^2$. The upper right panel shows the rate of the pole dominance, $B(M^2; s_{th})$. Without higher dimension terms, the rate is very small because of the lack of the low energy correlation. The lower panels show the mass in the left panel and residue in the right panel, respectively. The arrows indicate the M^2 values where the pole dominance ratio begins to fall below 50%, which is the upper bound of the Borel window. In the larger M^2 , both quantities show the moderate stability because of the pseudo peak behavior just below s_{th} .

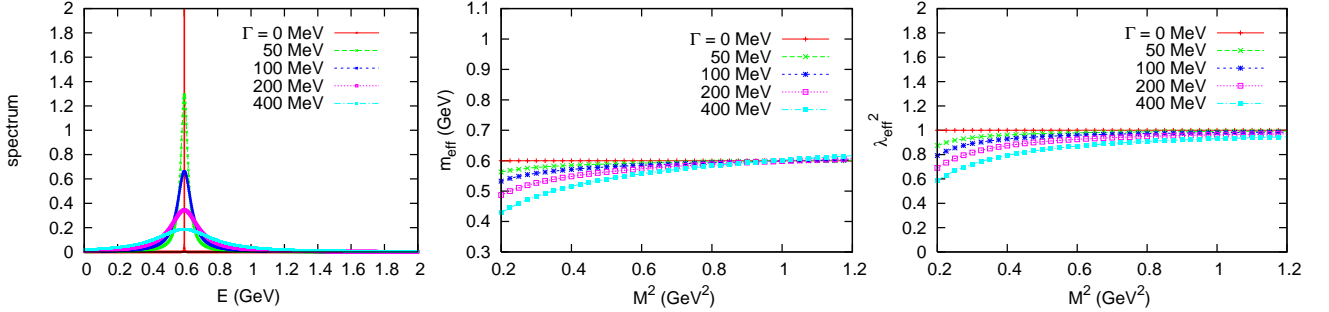


FIG. 2: (Color online) The relations among the Breit-Wigner form of the spectral function, the effective mass and the residue plots. The left panel shows the Breit-Wigner spectral function with the fixed mass 600 MeV and the values of the width are taken as 0, 50, 100, 200, and 400 MeV. The middle and right figures show the effective mass and residue calculated by Eqs.(8) and (9) with the Breit-Wigner spectral function, respectively. Because of the low energy tails, the effective mass and residue plots shift downward in the case of the small M^2 .

Wigner function (BWF),

$$\text{const.} \times \frac{\Gamma^2/4}{(\sqrt{s} - m)^2 + \Gamma^2/4}, \quad (13)$$

where m is the pole mass and Γ is the width. The const. will be taken to normalize the integral of this function to

1. We show in the first panel of Fig.2 the BWF with the pole mass fixed to 600 MeV and the width taken as 0, 50, 100, 200, and 400 MeV.

Let us see the behavior of the physical quantities as a consequence after the substitution BWF into $\text{Im}\Pi^<(s)$ of the Eqs.(8) and (9). The middle and right panels in Fig.2

show the effective mass and residue plots, respectively. In the case of the zero width approximation, both mass and residue plots show the complete independence on the variation of M^2 as expected. On the other hand, in the nonzero width cases, BWF has the tail both in the lower and higher energy around the pole mass, and then the effective mass shifts downward (upward) in the lower (higher) M^2 .

Fig.2 tells us that, if we consider the effect of the width in the effective mass plot, the best Borel stability does not necessarily give the best fit of the spectral function. This violation of the Borel stability due to the width affects how to select the E_{th} and the final results. In the zero width or very narrow width case, usually we can fix E_{th} to give the best Borel stability because the effective mass plots of the zero width case do not depend on the Borel mass M^2 . But in the case with a wider width, how should we fix E_{th} ?

If we assume the shape of the spectrum for the resonances, the effective mass plots obtained by QSR can be compared with those of the known spectrum, and we can choose E_{th} to achieve the better fit. This can be seen in the following example. Let us consider the ρ meson which has the mass $m_\rho = 770$ MeV and the width $\Gamma_\rho = 150$ MeV, and assume that the spectral function is given by the Breit-Wigner form. We show in Fig.3 the effective mass plots for the BWF with $m_\rho = 770$ MeV and $\Gamma_\rho = 0, 150$ MeV, and also the effective mass plot obtained by the QSR with the OPE given in the literature [28] with several thresholds $E_{th} = 1.1, 1.2, 1.3$ GeV. In the zero width approximation, $E_{th} = 1.1$ GeV is preferred within QSR analyses because the Borel stability is achieved in the effective mass plot best. In this case, the mass is read as 0.7 GeV from the Borel stability. Once the effects of the width is considered in the effective mass plot, we lose the reason to select E_{th} which gives the best stability. But, comparing the effective mass plot of the BWF with the 150 MeV width, we find that the case of $E_{th} = 1.2$ GeV, in which the stability is slightly worse than the $E_{th} = 1.1$ GeV case, is better to reproduce the effective mass plot for BWF with the 770 MeV mass and the 150 MeV width. In this way, we can estimate the threshold E_{th} and the resonance mass m . Nevertheless, for the scalar meson case, we do not know neither the shape of the spectral function nor the width of the resonance, *a priori*. Thus, we cannot definitely obtain the exact values of the threshold and the resonance mass. In this analysis, the resonance masses are estimated by assuming the zero width and the 400 MeV width with the BWF. Then we adopt the range between two masses as our result of QSR. As we will see below, the difference of these two mass is about 20%.

As seen in the above argument, for resonances with a wider width, it is more difficult to extract the resonance mass than the zero width state. The results unavoidably have some ambiguities from the assumption of the shape of the spectral function and the width. Nevertheless, we can still estimate physical quantities because

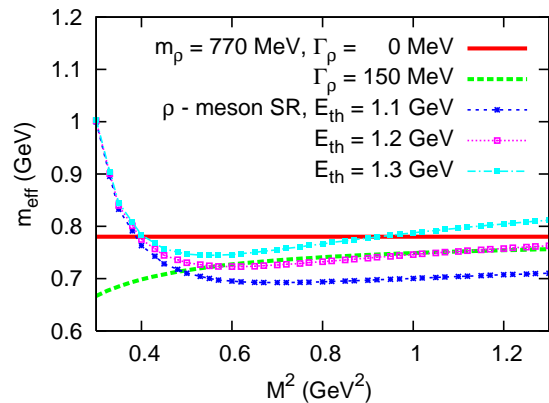


FIG. 3: (Color online) The effective mass for the Breit-Wigner function with $m_\rho=770$ MeV, $\Gamma_\rho=0, 150$ MeV, and for the ρ -meson SR results with $E_{th}=1.1, 1.2, 1.3$ GeV.

of the following two points: (i) As illustrated in Figs.2 and 3, although the width effects violate the stability of physical quantities, the stability is still moderate than naively expected even if we take relatively large widths, 400 MeV. Thus, even if the width exists, the usual determination of E_{th} may work as a first approximation. (ii) As an experience from QSR for mesons and baryons with small widths, QSR employing E_{th} taken around the position of the second resonances does satisfy the least sensitivity criterion. Since it is known experimentally that the continuous cross section begins from around second resonance, to fix E_{th} around the second resonance is reasonable and seems to be consistent with the philosophy of the quark-hadron duality. Therefore, we can expect the reasonable range of E_{th} using the experimental facts.

III. SU(3) SINGLET AND OCTET STATES IN THE CHIRAL SU(3) LIMIT

The σ meson may be realized as admixture of the flavor singlet and octet states, and the $f_0(980)$ meson will be its nonet partner of the flavor mixing in the flavor SU(3) symmetry breaking. It is important for the studies of the σ and $f_0(980)$ meson to know whether both resonances should be reproduced in the same footing and what makes the differences. For this purpose, we investigate quark flavor contents of the correlation functions for the flavor singlet and octet states in the SU(3) chiral limit, in which they decouple each other and we can investigate these states separately. In the SU(3) chiral limit, we will find that the splitting of the singlet and octet states stems only from the annihilation diagrams in which some quark lines are not connected between the space-time points x and 0 in the intermediate states of the correlation function. There are two types of the annihilation diagrams in the tetraquark case, the color singlet two quark state, $(q\bar{q})_1$, and the color octet quark with gluon, $(q\bar{q})_8G$. We will emphasize that the contributions

from the $q\bar{q}$ annihilation diagrams are more important in the tetraquark correlator than in two quark meson correlator.

A. Quark contents of the singlet and octet states

To study the quark contents of the light scalar nonets, it is convenient to introduce the diquark basis,

$$U = (\bar{d}\bar{s}), \quad D = (\bar{s}\bar{u}), \quad S = (\bar{u}\bar{d}), \quad (14)$$

which are anti-symmetrized in the color and flavor spaces. We do not specify the Lorentz structure in this section, since the flavor contents are the main issue here. The details of the interpolating fields will be given in Sec.IV A. In the tetraquark case, the quark content of the singlet state is described in the diquark basis as

$$\mathcal{S} = \frac{1}{\sqrt{3}}(U\bar{U} + D\bar{D} + S\bar{S}), \quad (15)$$

and for the octet states, for example, the quark contents are given by

$$\begin{aligned} \mathcal{O}_1 &= U\bar{D} \\ \mathcal{O}_2 &= \frac{1}{\sqrt{6}}(U\bar{U} + D\bar{D} - 2S\bar{S}), \\ \dots \end{aligned} \quad (16)$$

in a similar way to the quark contents of the usual $q\bar{q}$ meson cases.

The isodoublet κ and isovector a_0 belong to purely the octet because of the nonzero isospin, while the isoscalar σ and f_0 can be composed of the mixture of the singlet and octet states in the real world where the flavor SU(3) symmetry is broken by the quark masses. If the ideal mixing is realized, the σ and f_0 can be written as

$$\begin{aligned} \sigma &\sim (ud)(\bar{u}\bar{d}) = \bar{S}S = \sqrt{\frac{1}{3}}\mathcal{S} - \sqrt{\frac{2}{3}}\mathcal{O}_2, \\ f_0 &\sim \frac{1}{\sqrt{2}}[(us)(\bar{u}\bar{s}) + (ds)(\bar{d}\bar{s})] \\ &= \frac{1}{\sqrt{2}}[\bar{D}D + \bar{U}U] = \sqrt{\frac{2}{3}}\mathcal{S} + \sqrt{\frac{1}{3}}\mathcal{O}_2. \end{aligned} \quad (17)$$

From now on, we consider the chiral limit taking the zero quark masses. This limit is convenient to study the difference between the singlet and octet states. The study of the sigma meson in this work is valid even in the physical world with the finite strange quark mass, since, with the SU(3) breaking due to the strange quark mass, the ideal mixing is expected to be realized and the quark contents of the sigma meson is given by Eq.(17). In this case, the sigma meson consists only of the up and down quarks. For the f_0 and the octet mesons, it is important to include the finite strange quark mass.

We will find that important contributions for the difference between the singlet and octet states are the mixing of four-quark (4q) states with two-quark (2q) states, two-quark and gluon mixed (2qG) states or glueball states.

B. The annihilation diagrams in 2q-2q and 4q-4q correlators

As seen in Eqs.(17) and (18), the difference of the singlet and octet correlation functions is important to make the splitting of the σ and f_0 mesons. Here we would like to focus on the annihilation diagrams, since they are only the source of the splitting. We will also see that the annihilation diagrams play key roles especially for the scalar meson spectra. The remarkable point is that the effects of the annihilation diagrams are more important in the 4-quark correlators than the 2-quark mesonic correlators. This can be understood from the viewpoint of the momentum conservation. Here the annihilation diagram means the diagrams which have some quark lines disconnected between x and 0.

First of all, we start with discussion about the annihilation diagrams in the two-quark (2q-2q) correlators. Some typical OPE diagrams are shown in Fig.4. The dashed circles represent a pair of quarks to form the condensate. The perturbative diagrams shown in Fig.4 a) and b) contribute relatively high energy side of the correlation function. Diagram a) includes 1-loop without α_s corrections. Diagram b) is one of the annihilation diagrams, since the quark lines are not connected in the intermediate state. This diagram has three loops with α_s^2 correction and consequently it is strongly suppressed compared to diagram a). In diagram b) the two-gluon propagation is necessary because of the traceless property of the color SU(3) matrix. The suppression of this type of the diagrams can be also explained from large N_c counting [23]. The higher dimension terms shown in Fig.4 c) and d) contribute to the low energy side of the correlation function. Diagram c) is not the annihilation diagram since the quark lines are connected through the quark condensates. Diagram d) is very similar with diagram c), but the pairs of the quarks to form the condensate are different. Diagram d) is the annihilation diagram. However, this contribution vanishes at this $O(\alpha_s)$ order because of the color traceless properties. All of these facts suggest the strong suppression relative to the non-annihilation diagrams from low to high energy in the case of the 2q-2q correlators.

Next we turn to the discussion of the annihilation diagrams in the four-quark (4q-4q) correlators. We show in Fig.5 some examples of the diagrams in the 4q-4q correlators. Diagrams a) and b) are perturbative diagrams. Diagram b) is the annihilation diagram but it is suppressed by α_s^2 in the same way as the 2q-2q correlator case. Diagram c) is the leading annihilation diagram with $(q\bar{q})_1$ configuration. In contrast to the 2q-2q correlator cases, the $q\bar{q}$ annihilation diagrams can appear without gluon propagations, since the other two quarks can carry the momentum. Consequently no α_s suppression comes in. Diagram d) is also the annihilation diagram in dim.8 with the configuration $(q\bar{q})_8G$. This is not again suppressed by the α_s correction. Such annihilation diagrams can widely appear in the higher dimension terms. This means that the annihilation processes are much more important

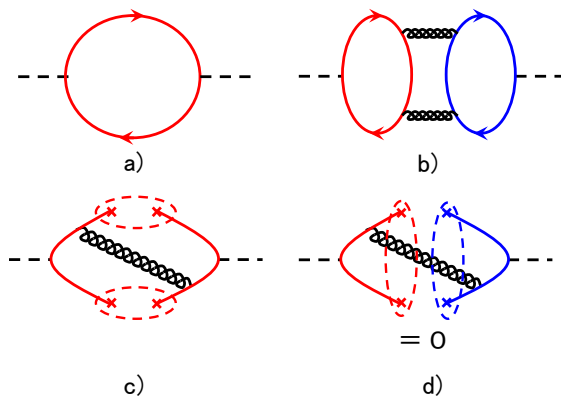


FIG. 4: (Color online) Some diagrams in the 2-q correlators. The flavor is distinguished by the line of color. a) The leading perturbative contribution in dim.0 term. b) The perturbative $q\bar{q}$ annihilation diagrams in dim.0 term with suppression factors, $1/N_c$ and α_s^2 . c) The leading power correction in dim.6 including $(q\bar{q})_s G$ configurations without annihilations. d) The $O(\alpha_s)$ power correction in dim.6 to the annihilation diagrams is vanished because of traceless properties of Gell-Mann matrix.

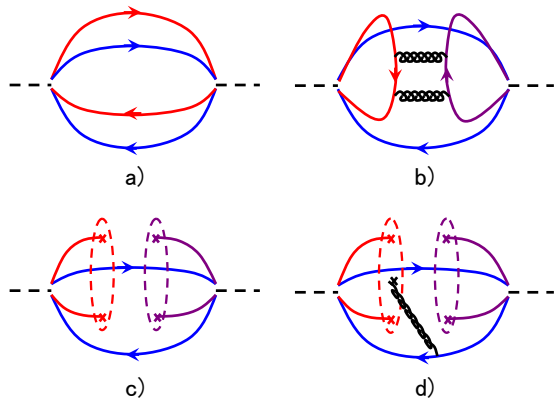


FIG. 5: (Color online) Some diagrams in the 4-q correlators. The flavor is distinguished by the line of color. a) The leading perturbative contribution in dim.0 term. b) The leading $q\bar{q}$ annihilation diagram in dim.0 term. c) The leading power correction in dim.6 to the annihilation diagrams including $(q\bar{q})_1$ configuration without α_s suppression factor. d) The annihilation diagrams in dim.8 which includes the configuration $(q\bar{q})_s G$.

in lower energies where we would like to investigate the properties of the scalar mesons.

Here we would like to stress that the annihilation processes do not directly imply 2q propagation emerged from tetraquark configuration. Indeed, as shown in Fig.6, the annihilation diagrams can represent either 2q s-channel propagation or 4q propagation with exchanging the resonance in the t-channel. Especially, contributions from the latter processes can be interpreted as diquark-diquark correlation in our tetraquark fields as product of diquark fields. We will see later that the annihilation diagrams

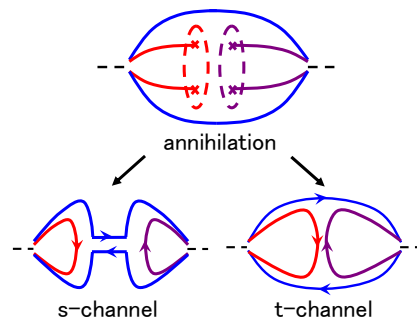


FIG. 6: (Color online) The two ways of interpretation of the annihilation diagrams. By deforming the quark line, we can interpret the annihilation diagrams as either 2q like s-channel propagation or 4q like t-channel propagation with exchange of mesonic resonances.

provide important contributions in our Borel analyses.

C. The splitting between singlet and octet states

Now we discuss how the annihilation diagrams studied in the previous subsection contribute to the flavor singlet and octet correlation functions. The flavor contents of the singlet and octet correlators are given respectively by

$$\frac{1}{3} \langle T[\bar{U}U(x)] [\bar{U}U(0) + \bar{D}D(0) + \bar{S}S(0)] \rangle + (\text{perm.}), \quad (19)$$

$$\langle T[\bar{U}D(x)] [\bar{U}D(0)] \rangle, \dots \quad (20)$$

where for the octet we use Eq.(16). These correlators consist of three types of correlators in terms of the flavor content:

$$[\bar{U}U(x)] [\bar{U}U(0)] = [ds\bar{d}\bar{s}(x)] [\bar{d}\bar{s}ds(0)], \quad (21)$$

$$[\bar{U}U(x)] [\bar{D}D(0)] = [ds\bar{d}\bar{s}(x)] [\bar{s}\bar{u}su(0)], \quad (22)$$

$$[\bar{U}D(x)] [\bar{U}D(0)] = [ds\bar{s}\bar{u}(x)] [\bar{d}\bar{s}su(0)]. \quad (23)$$

In the first expression, all the diquarks have the same flavor, the second expression is the correlation between the different flavor tetraquarks consisting a pair of the same flavor diquarks, and the third expression has two same tetraquarks which are made up of a pair of different diquarks. For the flavor singlet, the first two contribute, while for the octet only the last type of the correlators takes place.

Now we count possible configurations for the annihilation diagrams in each correlator shown above. Since neither QCD interaction nor vacuum condensates can change quark flavors, we can connect only the pair of the quark and antiquarks which have the same flavor. Thus, the first correlator (21) has both the four-quark connected diagrams like diagram a) in Fig.5 and the $q\bar{q}$

annihilation diagrams like diagram c) and d) in Fig.5:

$$ds\bar{d}\bar{s} \rightarrow ds\bar{d}\bar{s} \text{ (direct)}, \quad (24)$$

$$ds\bar{d}\bar{s} \rightarrow [(d\bar{d})_1, (d\bar{d})_8 G, G^2] \rightarrow ds\bar{d}\bar{s}, \quad (25)$$

$$ds\bar{d}\bar{s} \rightarrow [(s\bar{s})_1, (s\bar{s})_8 G, G^2] \rightarrow ds\bar{d}\bar{s}, \quad (26)$$

where we explicitly write down the possible color singlet configurations for the annihilation processes in the intermediate states. Here we have also mentioned the $q\bar{q}q\bar{q}$ annihilation process as G^2 in the intermediate state. This process gives 4q-gluon correlation. In leading α_s analysis up to dim.12, however, such $q\bar{q}q\bar{q} \rightarrow G^2$ diagrams do not appear. In the similar way, we find that the second type of the correlator (22) has only the annihilation diagrams:

$$ds\bar{d}\bar{s} \rightarrow [(s\bar{s})_1, (s\bar{s})_8 G, G^2] \rightarrow su\bar{s}\bar{u}. \quad (27)$$

The last correlator, which contributes to the octet, has both the four quark connected diagrams and the $q\bar{q}$ annihilation diagrams:

$$ds\bar{s}\bar{u} \rightarrow ds\bar{s}\bar{u} \text{ (direct)}, \quad (28)$$

$$ds\bar{s}\bar{u} \rightarrow [(d\bar{u})_1, (d\bar{u})_8 G] \rightarrow ds\bar{s}\bar{u}, \quad (29)$$

As we have mentioned, the first and second types of the correlators contribute to the singlet state, while the octet correlator has only the third one. From these observations, now we can see the singlet state has much more annihilation diagrams, or 4q-2q correlation effects than the octet states. In fact, the explicit calculation given in the Appendix.A shows the number of the $q\bar{q}$ annihilation diagrams is larger in singlet than in octet by factor 4.

IV. THE BOREL ANALYSES

In this section, we perform the Borel analyses for the σ meson and also the scalar states with the flavor singlet and octet in the flavor SU(3) limit. We first discuss the interpolating fields used in these analyses in subsection IV A. There we introduce linear combinations of the interpolating fields constructed by the scalar and pseudoscalar diquarks with a mixing angle θ . We also discuss the criterion to determine the interpolating fields based on the argument for the Borel window given in subsection II A. In subsection IV B, we show the results for the flavor singlet and octet states. Subsection IV C is devoted to discussion for the result of the σ meson. There we will find that the correlation function in the Borel analysis shows large contributions around $E = 600 \sim 800$ MeV.

Throughout our analyses, we use the standard values of the condensates in OPE: $\langle \bar{q}q \rangle = -(0.230 \text{ GeV})^3$, $\langle \bar{q}q_s \sigma Gq \rangle / \langle \bar{q}q \rangle = 0.8 \text{ GeV}^2$, $\langle \frac{\alpha_s}{\pi} G^2 \rangle = 0.012 \text{ GeV}^4$ and $\alpha_s(1\text{GeV}) = 0.4$. The OPE is evaluated within the factorization hypothesis without quantum loop corrections. The detail of the OPE calculation is given in Appendix.A.

A. Interpolating fields

In QSR, it is technically important to use such good interpolating fields as to pick up largely the resonance state and have smaller correlation with the higher energy states. With the number of quarks increasing, there are several choices of the local interpolating fields with the quantum number of our interest in contrast to the $q\bar{q}$ meson cases. The authors of Ref.[22] comprehensively studied the possible local interpolating fields of the tetraquark and the properties of the scalar mesons by constructing QCD sum rules with OPE up to dim.8. In this work, we calculate the OPE of the correlation function up to dim.12, considering linear combinations of the following two operators for the σ meson:

$$J_P = \epsilon^{abc} \epsilon^{dec} [u_a^T C d_b] [\bar{u}_d C \bar{d}_e^T], \quad (30)$$

$$J_S = \epsilon^{abc} \epsilon^{dec} [u_a^T C \gamma_5 d_b] [\bar{u}_d \gamma_5 C \bar{d}_e^T], \quad (31)$$

where a, b, c, \dots represent the color indices, ψ^T means the transposed spinor of ψ and C is the charge conjugation matrix. The above interpolating fields, J_P and J_S , are constructed by two pseudoscalar diquarks and two scalar diquarks, respectively. The linear combination is given with a mixing angle θ ($0 \leq \theta < \pi$) by

$$J(\theta) = \cos \theta J_P + \sin \theta J_S. \quad (32)$$

The mixing angle θ in the interpolating field (32) is determined so that the interpolating field couples more strongly to the resonance state and have less contributions from the higher energy states and scattering background, which is achieved by imposing the following criteria:

- a). Sufficiently wide Borel windows are established in the sum rule.
- b). The effective masses and residua are weakly dependent on the Borel mass M^2 as much as possible.
- c). The results have also adequately weak dependence on the threshold E_{th} .
- d). The effective residua are satisfactorily large.

These criteria are not independent each other and the mixing angle can be insensitive to some of them. Hence, the mixing angle is not uniquely fixed in quantitative manner. Here we discuss typical mixing angles which simultaneously satisfy the above criteria with better degree. In the followings, we explain the meanings of the criteria separately and understand the priorities among these criteria.

The criterion **a)** is most important, being essential to avoid the pseudo peak artifacts and reduce truncation errors of the OPE, as emphasized in Sec.II A. Thus, this criterion should be always satisfied independently of the other criteria to guarantee the sum rules contain largely contributions from low energy physics.

After we find the Borel window in the sum rules, the next task is to establish better pole isolation from the background contamination, which can be done by satisfying the criteria **b)** and **c)**. The background contamination comes mainly from scattering states of two mesons and other resonance states. In the low energy side, scattering states of two Nambu-Goldstone bosons, i.e., $\pi\pi$, KK , $\eta\pi$, scattering states can appear from $E = 0$ in the present analyses because all the Nambu-Goldstone bosons are massless in the chiral limit. If these states largely contribute to the sum rules, the effective residue and mass obtained in the sum rules have larger M^2 dependence in the M^2 region below the resonance pole than we expect from the resonance width, which has been discussed in Sec.II C. This contamination below the resonance pole can be reduced by the selection of θ with satisfying the criterion **b)** well. The background contamination above the pole energies comes from higher excited resonance states and meson scattering states other than the Nambu-Goldstone bosons. In the case that such contamination is large, the physical quantities have large dependence against the variation of E_{th} . This can be reduced by imposing the criterion **c)**.

The criterion **d)** is imposed to have the large overlap of the interpolating field with the resonance pole and to reduce the truncation errors of OPE. In our analyses, we neglect higher-dimensional terms of OPE than the dim.12 terms. If the residua obtained in the sum rule are sufficiently large, the interpolating fields used in the analyses have enough overlaps to the resonance states and the sum rules constructed with the approximated OPE may contain so much information for the resonance to be extracted. But, if the obtained residua are small, the neglected higher-dimensional terms might have important information on the resonance states, although the OPE convergence is well provided. Thus, we consider the criterion **d)**. Nevertheless, the criterion **d)** has less priority than the criteria **b)** and **c)**. This is because the best choice of θ is not always the one which have the largest overlap with the region below E_{th} . Even if the low energy correlation is large, it can be just a signal of strong contamination from the background. Therefore, the most important thing is that we construct the sum rules within the sufficiently wide Borel window satisfying the criterion **a)** with the best choice of the interpolating field which have the least overlap with the background.

B. Borel analyses of flavor singlet and octet states

Let us consider the flavor singlet and octet states produced by the interpolating fields given in Eq.(32) with the mixing angle θ and having the quark contents (15) and (16). The mixing angle is determined by the criteria discussed in Sec.IV A. The detailed discussions and the technical issues are given in Appendix.B. Our findings for the mixing angle are as follows:

- the Borel windows can be established in all the mix-

ing angles except $\theta \sim 0$ for the flavor octet case.

- the results for the physical quantities are not very sensitive to the choice of the mixing angle θ except some region of θ both in the flavor singlet and octet cases.
- one of the best value of the mixing angle both for the singlet and octet is $\theta \simeq 7\pi/8$. Thus in this section we will show the results for $\theta = 7\pi/8$.
- the residua of the singlet states have larger values than those of the octet states in almost all region of θ .
- the effective masses of the octet case are typically smaller than those of the singlet, and the Borel stability is worse in the octet case.

The last two findings may imply, in comparison to the singlet case, that the octet interpolating field used here does not have sufficiently large overlap with the resonance state or that the width of the resonance in the octet channel is considerably large. For further investigation of the octet states, it might be necessary to use interpolating fields with different Lorenz structure.

Hereafter we proceed to discussions of the Borel analyses of the scalar mesons with fixing the mixing angle as $\theta = 7\pi/8$. First of all, we examine the OPE convergence of the pole dominance, which are important to establish the appropriate Borel window, and we emphasize importance of the higher dimension terms. Here we fix the threshold to a typical value $E_{th} = 1.0$ GeV. We show in Fig.7 the OPE dependence of the ratio of the pole contribution to the whole spectral function $B(M^2; s_{th})$ defined in Eq.(11) for singlet and octet cases. We can see that the OPE corrections to the perturbative term (dim.0) is extremely important to achieve the pole dominance. It can be also seen in Fig.7 that the higher dimension terms than dim.8 is not so important for the pole dominance. Nevertheless, as seen in the plots of the effective masses (Fig.8), the dim.10 and 12 terms are important to obtain the Borel stability in the small M^2 region (typically $M^2 < 1.0$ GeV² $\sim M_{\max}^2$) where we will evaluate the physical quantities later. This means that these higher dimension terms have essential to reproduce the low energy resonances. For the singlet case, the dim.12 term improves the Borel stability well, while in the effective mass for the octet state the dim.10 and 12 terms do not help as well as the singlet case. The Borel stability obtained with including only the dim.0 term can be interpreted as the artificial stability discussed in Sec.II B, since the pole dominance is not achieved in these cases. As emphasized in Sec.III C, the difference of the effective masses of the singlet and octet comes from the annihilation diagrams, which is increasingly important in higher dimension terms or low energy region.

Next we evaluate the resonance masses and residua for the flavor singlet and octet states in the chiral limit. We calculate the masses and residua widely with several

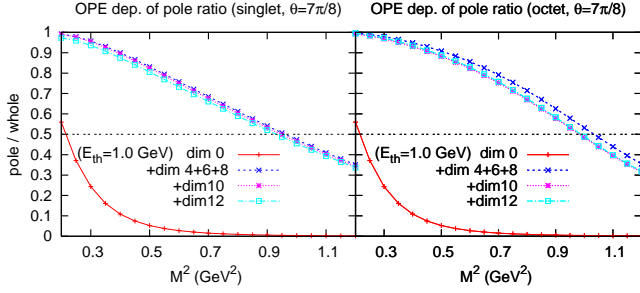


FIG. 7: (Color online) The OPE truncation dependence of the pole dominance, $B(M^2; s_{th})$, for singlet and octet case with the threshold $E_{th} = 1.0$ GeV.

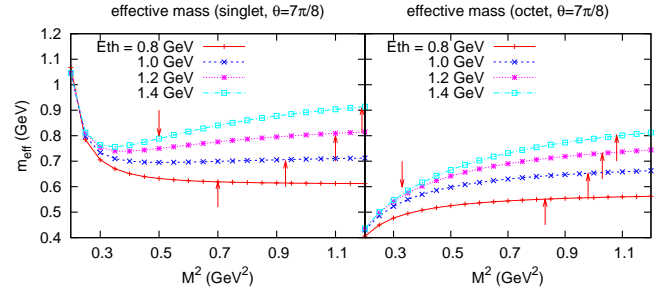


FIG. 9: (Color online) The effective masses for the singlet and octet states. The values of the threshold E_{th} are 0.8, 1.0, 1.2 and 1.4 GeV. The downward and upward arrows indicate the lower and upper bounds of the Borel window, respectively.

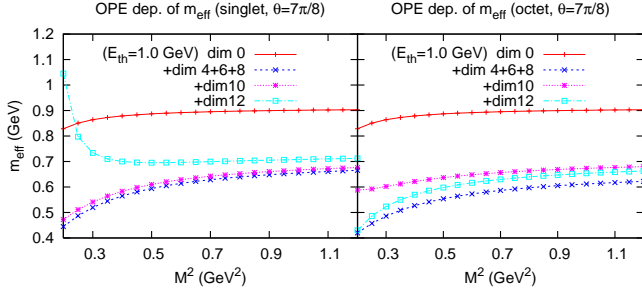


FIG. 8: (Color online) The OPE truncation dependence of the effective masses for singlet and octet case with the threshold $E_{th} = 1.0$ GeV.

values of $E_{th} = 0.8, 1.0, 1.2,$ and 1.4 GeV, in order to see the threshold dependence discussed in Sec.IV A and the effect of the resonance width studied in Sec.II C. We show in Fig.9 the plots of the effective mass for singlet and octet states with $E_{th} = 0.8, 1.0, 1.2,$ and 1.4 GeV. The downward and upward arrows indicate the lower and upper bounds of the Borel window, respectively. The way to fix the Borel window has been given in Eqs.(10) and (11). The lower Borel mass is not dependent on the threshold, since it is determined only by the OPE convergence.

We extract the masses of the scalar mesons from the effective mass plot in Fig.9 with consideration of its possible modifications from the resonance width, as discussed in Sec.II C. For the singlet state, we find the moderate Borel stability for $E_{th} = 1.0 \sim 1.4$ GeV in Fig.9. This would imply that some resonance state saturate the spectral function around $E \sim 700$ MeV. We estimate the mass for the singlet state at 700 MeV for a small width state, finding almost perfect Borel stability with $E_{th} = 1.0$ GeV. If the state has some larger width, we evaluate the mass by 850 MeV with a possible width 400 MeV according to the discussion in Sec.II C, in which we found that the Borel stability is not perfectly achieved in the case of the resonance with width. Finally we conclude that the present QCD sum rule estimate the flavor singlet scalar meson by $700 \sim 850$ MeV with consideration

of the possible width up to 400 MeV.

For octet state, we estimate the resonance mass at $600 \sim 750$ MeV in the similar way to the singlet case. Nevertheless, the effective mass in the octet channel depends on the Borel mass fairly. One of the possible explanations is that the signal of the octet resonance is weak and considerably affected by low energy scattering states. Another possibility is that the observed state has the large width, let us say, $100 \sim 400$ MeV, which can be estimated from the comparison to the effective mass of the Breit-Wigner form in Fig.2. Probably both effects may play important roles in the octet sum rules.

We also plot the effective residua for the singlet and octet cases in Fig.10. The Borel stability is achieved as similarly as that of the effective mass. The residua for single and octet states are evaluated by $(20 \sim 35) \times 10^{-7} \text{ GeV}^8$ and $(7.5 \sim 13) \times 10^{-7} \text{ GeV}^8$, respectively. The overlap strength of the singlet case is factor $2 \sim 3$ larger than the octet state.

Both in the singlet and octet states, the threshold dependence is not very small. This would suggest the separation between resonance pole and threshold would not be completely done. For the further investigation, we would need more elaborated technique to isolate the resonance states, for instance, large N_c argument as discussed in Ref.[27].

C. Borel analysis for sigma meson

We discuss the Borel analysis for the σ meson in the chiral limit. With the SU(3) breaking, the ideal mixing of the flavor singlet and octet components may be realized and the lighter scalar meson with $I = 0$ and $S = 0$, namely the σ meson, may be described by only the up and down quarks. (The ideal mixing is the assumption in this work. To check this assumption, we need to investigate the flavor mixing angle in QCD sum rules with a finite strange quark mass.) For the ideal mixing, the spectral function for the σ meson is given by a linear combination of the singlet and octet spectral functions in the chiral

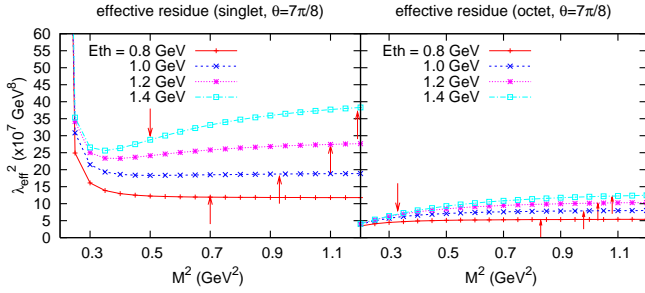


FIG. 10: (Color online) The effective residues for the singlet and octet states. The values of the threshold E_{th} are 0.8, 1.0, 1.2 and 1.4 GeV. The downward and upward arrows indicate the lower and upper bounds of the Borel window, respectively.

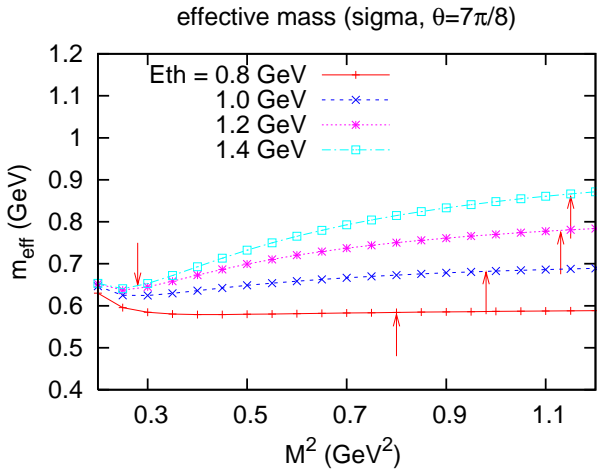


FIG. 11: (Color online) The effective mass for the σ meson. The values of the threshold E_{th} are 0.8, 1.0, 1.2 and 1.4 GeV. The downward and upward arrows indicate the lower and upper bounds of the Borel window, respectively.

limit:

$$\langle T J_\sigma \bar{J}_\sigma \rangle = \frac{1}{3} \langle T J_S \bar{J}_S \rangle + \frac{2}{3} \langle T J_O \bar{J}_O \rangle. \quad (33)$$

We work again with $\theta = 7\pi/8$ for the mixing angle of the interpolating field.

Evaluating the effective mass and residue of the sigma meson, we obtain the plots with $E_{th} = 0.8, 1.0, 1.2$ and 1.4 GeV in Figs.11 and 12. In these plots, we find again fairly good Borel stability both for the effective mass and residue. In the same way as the flavor singlet case, we estimate the resonance pole mass at $600 \sim 800$ MeV with paying attention to the possible width ~ 400 MeV. The pole residue is also evaluated by $(10 \sim 20) \times 10^{-7} \text{ GeV}^8$. The value of the residue is consistent with the expectation that it is a superposition of the singlet and octet states with group theoretical weights for the ideal mixing, which are $1/3$ and $2/3$ for the singlet and octet contribu-

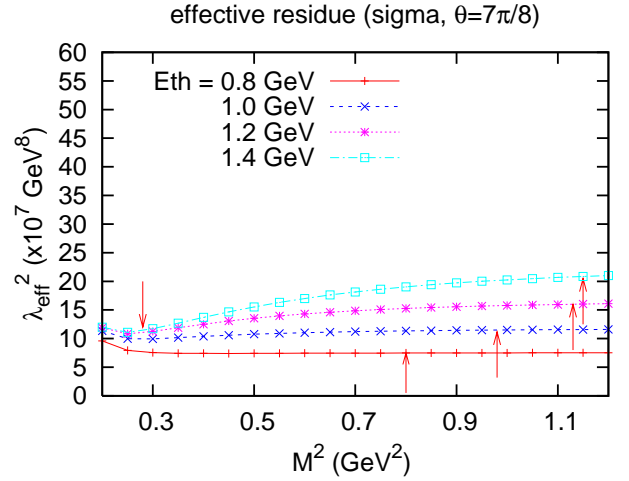


FIG. 12: (Color online) The effective residue for the σ meson. The values of the threshold E_{th} are 0.8, 1.0, 1.2 and 1.4 GeV. The downward and upward arrows indicate the lower and upper bounds of the Borel window, respectively.

tions, respectively.

This σ mass obtained in the present sum rule analysis with the tetraquark operator is considerably smaller than that extracted from correlator analyses with the two-quark operators, which is ~ 1.2 GeV. As discussed in Sec.IV B, the 2q operator mainly couples to the 2q components, while the tetraquark operators induce both the 4q components and the considerable 2q and 2qG components. The present tetraquark investigation shows that that inclusion of 4q and 2qG components is relevant to explain the smaller σ mass [24].

As a whole, finding the wider Borel window in the sigma meson sum rule, we conclude that the results for the σ meson is more reliable than the singlet and octet cases. Especially it is notable that the lower bound of the Borel mass is sufficiently small. This helps us to investigate low energy contributions for the σ channel. Due to the small lower bound of the Borel mass and the Borel stability obtained even in $M^2 = 0.3 \text{ MeV}^2$, we conclude that the pole dominance of the σ resonance is fairly established with small contamination of low energy scattering. We also see that the large strength comes mainly from the flavor singlet component, which shows the large enhancement around $E = 700 \sim 850$ MeV region.

In closing this section, we would like to emphasize that, although having some ambiguities coming from the influence of the scalar meson width on the Borel stability and the choice of the mixing angle θ , the present QSR analyses with the tetraquark operators provide the scalar meson masses less than 1 GeV, which cannot be produced in QSR with 2q operators.

V. DISCUSSION

The present QSRs are constructed in the SU(3) chiral limit. It is very interesting to extend our QSRs beyond the chiral limit with a realistic strange quark mass. Especially for realistic calculation of the masses of the octet scalar mesons, such as κ and a_0 , inclusion of the strange quark mass is absolutely necessary. It is also interesting to investigate the mixing angle of the flavor singlet and octet interpolating fields with finite strange quark mass. In this work, we have assumed the ideal mixing for the flavor content of the σ meson operator. But it is not trivial to realize the ideal mixing in the physical scalar meson nonet. Analyses with the strange quark mass for the flavor mixing angle is possible within the QSR approach. This would clarify the strange contents of the σ meson.

Inclusion of the quark masses with the SU(3) symmetric way is also a good theoretical issue. In the present analyses we have found that contributions from the annihilation diagrams are responsible for the splitting of the singlet and octet states. It is good to know the quark mass effects on the splitting. Especially, in the chiral limit, we have found that the octet tetraquark operator weakly couples to the physical state, so that it is interesting to investigate how the octet state changes with the finite quark mass.

The issue of the flavor mixing angle and splitting of the singlet and octet states is closely related to the mass difference of the f_0 and a_0 . In the present experiments they almost degenerate. The a_0 meson may be classified into the flavor octet, while the f_0 meson may be described by a linear combination of the singlet and octet operators with the flavor SU(3) breaking. Thus the mass difference is given by the mixing angle and contributions of the annihilation diagrams in the QSR approach. It is interesting to study how the degeneracy of f_0 and a_0 is realized in QSR.

In this work, we have used the tetraquark operators with expectation to have strong coupling to the four-quark states and some contributions from the two-quark (2q) and two-quark-one-gluon (2qG) states. It is also interesting to investigate the scalar meson states using the operators having large overlap with two-quark states and small coupling with four-quark states and to compare this with the present analyses. It has been reported in Ref.[8] that κ and a_0 may have large components of two-quark states rather than four-quark states and the coupling of the two-quark states with nonresonant scattering states makes the κ and a_0 masses lighter in a similar way to the Feshbach resonances. In fact, the previous QSR studies with two-quark mesonic currents for $\kappa(800)$ and $a_0(980)$ showed $1.0 \sim 1.2$ GeV and this is not too higher than the experimental value. It would be natural to develop the ideas that the 2q state with some additional components might lead the experimental mass. In future, we will report the analysis using such operator with the help of the large N_c argument [27].

In order to investigate further the widths of the scalar meson states, it is necessary to investigate three point correlation functions for the $\sigma \rightarrow \pi\pi$, for instance. To obtain the decay width in QSR, we need to calculate both the two-point and three-point correlation functions, and to perform combined analyses of them in self-consistent ways to determine the mass, the residue, the threshold and the mixing angle.

It is also interesting to calculate two photon decays of the scalar mesons in QSR in order to compare mesonic molecule pictures. It has been reported in Ref.[26] that the $K\bar{K}$ molecule picture of the f_0 and a_0 mesons proposed by Ref.[25] provides a factor 3 larger decay rate of $a_0 \rightarrow \gamma\gamma$ than experiments and also that two quark picture predicts much larger decay rates of $a_0 \rightarrow \gamma\gamma$ and $f_0 \rightarrow \gamma\gamma$. The discrepancy could be explained by the tetraquark picture, since decay of four quarks into two photons may be suppressed compared to two quarks to two photons by the electromagnetic constant α and the quark wavefunction $|\Psi(0)|^4$ at the origin.

It is an important question whether correlation function analyses with local operators, such as the present QSR, can reproduce nature of spatially extended objects like mesonic molecular states. The correlation functions observe overlaps of the local operators and the physical states. In principle, if the overlap is not extremely small, the correlation functions have components of the molecular states. However, it is not sufficient at all to investigate the nature of the physical states only from the overlap of the local operators and the physical states. We certainly need other information of the wavefunctions, such as the decay widths.

VI. SUMMARY

In this paper, we discuss the properties of the $\sigma(600)$ meson in the QCD sum rules (QSR) for the tetraquark operators, emphasizing the importance of setting up the Borel window to avoid artificial Borel stability. The flavor structure of the sigma interpolating field is given by the SU(3) singlet and octet representations assuming the ideal mixing with the SU(3) flavor breaking. We investigate also the flavor SU(3) singlet and octet states for the light scalar meson with $I = 0$ and $S = 0$ in the massless limit with special attentions for the roles of the constituents of the σ meson. Having shown that the splitting between the singlet and octet states stems from the annihilation diagrams in which only two quark lines out of four carry the hard momenta, we have found that the contributions from the annihilation diagrams are responsible for the mass of the σ state around $600 \sim 800$ MeV, which is much lighter than the mass extracted by QSR with the two quark operators.

Investigation of the scalar meson in the present QSR have been carried out using the correlation functions for a linear combination of the tetraquark operators made up by the scalar and pseudoscalar diquarks. The mixing

angle has been determined with QSR so as to achieve better resonance isolation from the background contamination. We have also discussed possible influence of the large width of the scalar meson on the Borel stability.

For the singlet state, having found fairly good Borel stability within the practical Borel window, we have obtained the mass as $700 \sim 850$ MeV with considerations for the ambiguities coming from the possible width of the scalar meson and small dependence on the threshold parameter. For the octet state, we have found rather poor Borel stability and obtained a bit lighter mass around $600 \sim 750$ MeV with smaller coupling strength than the singlet case. This would suggest that, in the octet channel, the signal of the resonance state is rather small compared to background scattering states of two Nambu-Goldstone bosons, or that the resonance state has the large width. The present analyses have been done in the SU(3) chiral limit. It is interesting to investigate the octet state beyond the chiral limit with a realistic strange quark mass for the κ and a_0 mesons.

For the σ meson, having found wider Borel window and more Borel stability than the flavor singlet and octet cases, we have estimated the resonance mass at $600 \sim 800$ MeV and the residue at $(10 \sim 20) \times 10^{-7} \text{ GeV}^8$, which include again the ambiguities of the width and the choice of the threshold. Although the present analyses have some ambiguities coming from the influence of the physical width of the scalar meson on the Borel stability and the choices of the threshold and the mixing angle, we conclude that the QSR with the tetraquark operators provides the resonance masses of $600 \sim 800$ MeV in the σ meson channel in the chiral limit. This suggests that the σ meson has largely the four-quark components, since the QSR with the 2q operators cannot produce masses less than 1 GeV in the scalar channel.

Acknowledgments

We thank Professor H. Suganuma for helpful discussions. This work is supported by the Grant-in-Aid for the 21st Century COE ‘‘Center for Diversity and Universality in Physics’’ from the MEXT of Japan and in part by the Grant for Scientific Research (No. 18042001). This research is part of Yukawa International Program for Quark-Hadron Sciences.

APPENDIX A: THE OPE RESULTS

In this appendix, we present the expression of each term of the OPE for the correlation function (2) with the interpolating field (32) having the mixing angle θ ($0 \leq \theta < \pi$):

$$J(\theta) = \cos\theta J_P + \sin\theta J_S \quad (\text{A1})$$

The interpolating fields with specific mixing angles have definite chiral representations: $J(3\pi/4)$ is classified into

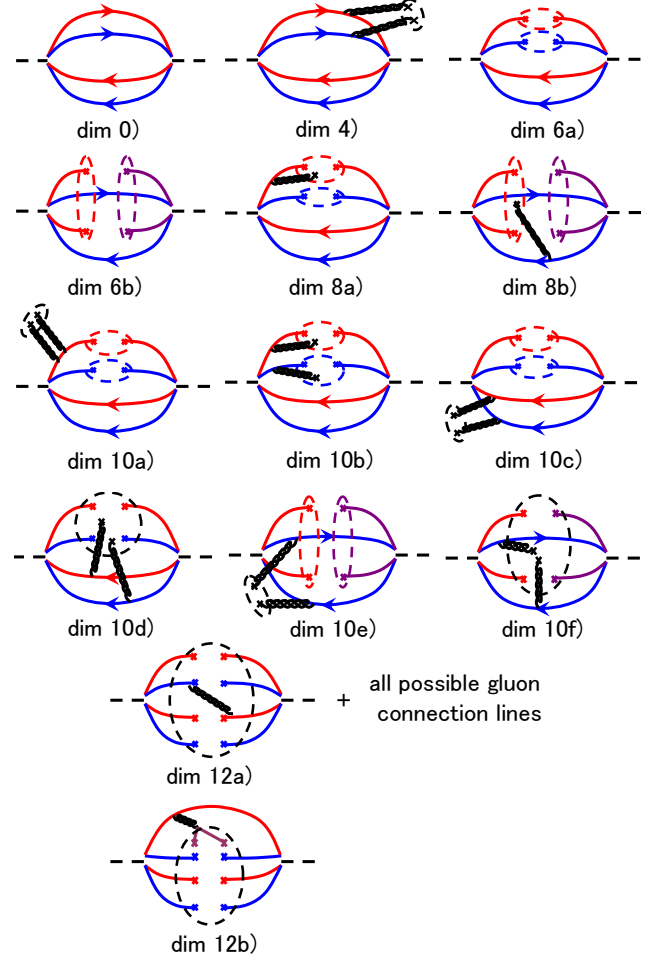


FIG. 13: (Color online) The diagrams for the OPE.

the irreducible representation $[(\mathbf{3}, \bar{\mathbf{3}}) \otimes (\bar{\mathbf{3}}, \mathbf{3})]$ of the chiral $SU(3)_L \otimes SU(3)_R$ group, while $J(\pi/4)$ is a combination of the $[(\mathbf{8}, \mathbf{1}) \otimes (\mathbf{1}, \mathbf{8})]$ and $(\mathbf{1}, \bar{\mathbf{1}})$ representations. (Actually $J(\pi/4)$ is classified into the nonet $[(\mathbf{9}, \mathbf{1}) \otimes (\mathbf{1}, \mathbf{9})]$ representation of the $U(3)_L \otimes U(3)_R$ group.)

The OPE of the correlation function is expressed by the coefficients C_i :

$$\Pi_i^{ope}(q^2) = \sum_{j=0}^4 C_{2j} (q^2)^{4-j} \log(-q^2) + \sum_{j=1}^{\infty} \frac{C_{8+2j}}{(q^2)^j}. \quad (\text{A2})$$

The relevant diagrams to calculate the OPE are shown in Fig.13.

We use $c \equiv \cos\theta$, $s \equiv \sin\theta$, and $\langle \bar{u}u \rangle = \langle \bar{d}d \rangle = \langle \bar{s}s \rangle = \langle \bar{q}q \rangle$ for the simplification of the OPE expressions. We also define N as a number of the annihilation diagrams, $N = 1$ (for octet), $N = 2$ (for σ) and $N = 4$ (for singlet).

For the terms from dim.0 to dim.4, we have

$$C_0 = -(c^2 + s^2) \frac{1}{2^{12} 3 5 \pi^6}, \quad (\text{A3})$$

$$C_4 = -(c^2 + s^2) \frac{\langle \frac{\alpha_s}{\pi} G^2 \rangle}{2^{10} 3 \pi^4} \times 2, \quad (\text{A4})$$

where “ $\times \dots$ ” is the multiplication factor from the permutation of diagrams.

From dim.6, the annihilation diagrams begin to appear. The dim.6 terms are calculated as

$$C_{6a} = (c^2 - s^2) \frac{\langle \bar{q}q \rangle^2}{2^3 3 \pi^2} \times 2, \quad (\text{A5})$$

$$C_{6b} = -(c^2 + s^2 - 2sc) \frac{\langle \bar{q}q \rangle^2}{2^5 3 \pi^2} \times N, \quad (\text{A6})$$

where the suffix of C stands for the diagram in Fig.13.

The dim.8 terms provide most important contributions. These are the first contributions beyond the polynomial $s^n (n > 0)$ and give the most of the low energy correlation. They are calculated as

$$C_{8a} = -(c^2 + s^2) \frac{\langle \bar{q}q \rangle \langle \bar{q}g_s \sigma Gq \rangle}{2^4 3 \pi^2} \times 4, \quad (\text{A7})$$

$$C_{8b} = -(c^2 + s^2 - 2sc) \frac{\langle \bar{q}q \rangle \langle \bar{q}g_s \sigma Gq \rangle}{2^6 3 \pi^2} \times 2N. \quad (\text{A8})$$

Note that the annihilation diagrams can give substantial contributions roughly $\sim 40\%$ of the total of dim.8.

From dim.10, the OPE begins to converge, but still substantial contributions give to the correlation function. The coefficients of the dim.10 terms are obtained as

$$C_{10a} = (c^2 - s^2) \frac{\langle \bar{q}q \rangle^2 \langle \frac{\alpha_s}{\pi} G^2 \rangle}{2^3 3^3} \times 4, \quad (\text{A9})$$

$$C_{10b} = (c^2 - s^2) \frac{\langle \bar{q}g_s \sigma Gq \rangle^2}{2^6 3 \pi^2} \times 2, \quad (\text{A10})$$

$$C_{10c} = (c^2 - s^2) \frac{\langle \bar{q}q \rangle^2 \langle \frac{\alpha_s}{\pi} G^2 \rangle}{2^4 3^2 \pi^2} \times 2, \quad (\text{A11})$$

$$C_{10d} = (c^2 - s^2) \frac{11 \langle \bar{q}g_s \sigma Gq \rangle^2}{2^{10} 3^2 \pi^2} \times 2, \quad (\text{A12})$$

$$C_{10e} = -(c^2 + s^2 - 2sc) \frac{\langle \bar{q}q \rangle^2 \langle \frac{\alpha_s}{\pi} G^2 \rangle}{2^5 3^2} \times N, \quad (\text{A13})$$

$$C_{10f} = -(c^2 + s^2 - 2sc) \frac{\langle \bar{q}g_s \sigma Gq \rangle^2}{2^9 3 \pi^2} \times N. \quad (\text{A14})$$

In our analysis, we calculate the OPE up to dim.12, because further dimension terms have no large enhancement factor of $\sim (4\pi)^2$ coming from cutting quark loops [20]. There are many diagrams for the dim.12 terms because we have many ways to attach the gluon line to the quark lines. The results after adding the all possible diagrams are

$$C_{12a} = \frac{\pi \alpha_s \langle \bar{q}q \rangle^4}{3^2} \quad (\text{A15})$$

$$\times [8(c^2 + s^2) - 3N(c^2 + s^2 - 2sc)], \quad (\text{A16})$$

$$C_{12b} = \frac{2^4 \pi \alpha_s \langle \bar{q}q \rangle^4}{3^5} [2(c^2 - s^2) - N(c^2 - sc)]. \quad (\text{A17})$$

There are no terms having the structure other than the above, such as $\langle \bar{q}q \rangle \langle \bar{q}g_s \sigma Gq \rangle \langle \frac{\alpha_s}{\pi} G^2 \rangle$.

APPENDIX B: θ DEPENDENCE OF THE EFFECTIVE RESIDUE AND MASS

In this Appendix, we discuss the detail of the θ dependence. We would like to draw a rough sketch of the allowed region for the mixing angle to achieve wider Borel window and better pole isolation following to the discussion in Sec.IV A.

We show in Fig.14 the effective mass obtained by the QSR as functions of the mixing angle θ ($0, 2\pi/8, 5\pi/8, 7\pi/8$) and the Borel mass M^2 . The threshold is taken as $E_{th} = 0.8, 1.0, 1.2, 1.4$ GeV in the same way as subsection IV B and IV C. We also show the effective residue in Fig.15 with the same θ and E_{th} as the effective mass plots.

The essential points were already mentioned in subsection IV B. Here we give more detailed explanations.

- the Borel windows can be established in all the mixing angles except $\theta \sim 0$ for the flavor octet case. For $\theta \sim 0$, the spectral condition $\text{Im}\Pi^{ope}(s) \geq 0$ is slightly violated unless we take E_{th} as large as ~ 2.0 GeV. Thus the region around $\theta = 0$ was avoided in subsection IV B to compare singlet and octet cases in the region where sum rules for both cases well satisfy the criteria in subsection IV A .
- the results for the physical quantities are not very sensitive to the choice of the mixing angle θ in the regions of $\theta = 0 \sim 2\pi/8$ and $6\pi/8 \sim \pi$ both in the flavor singlet and octet cases. This is most clearly reflected in the effective residue plots in Fig.15. On the other hand, except these regions, the effective residua strongly depend on the mixing angle and the threshold. We interpret that these strong dependences are mainly related to contributions from scattering states. This is because the residua in these θ regions show the large E_{th} dependence, which indicates that the resonance pole is not isolated enough.
- one of the best value of the mixing angle both for the singlet and octet is $\theta \simeq 7\pi/8$. If we consider only the singlet and σ meson cases, the best result is obtained with $\theta = 0$. In this case, the threshold dependence is extremely small, and we can expect that there are small contaminations in the region from resonance pole to E_{th} , i.e., the resonance is isolated.
- the residua of the singlet states have larger values than those of the octet states in almost all region of θ .
- the effective masses of the octet case are typically smaller than those of the singlet, and the Borel stability is worse in the octet case.

Effective mass plot

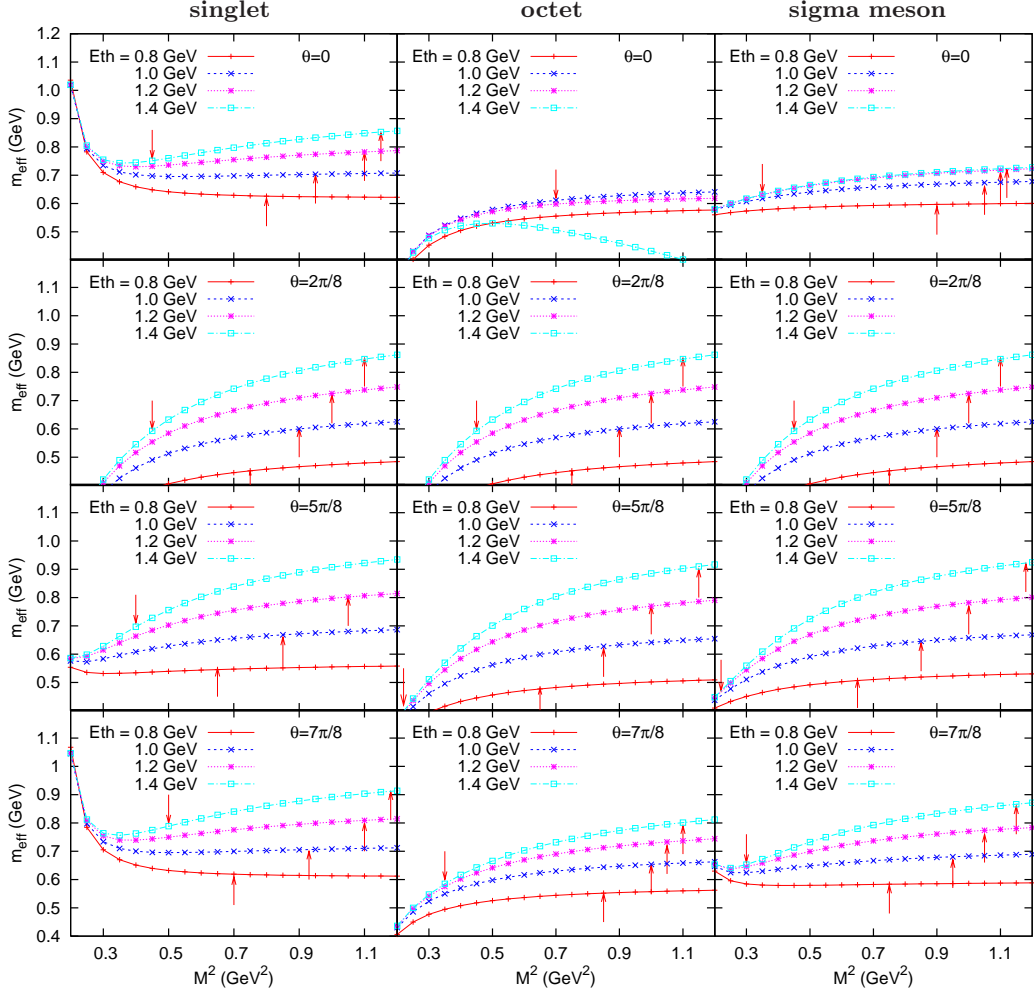


FIG. 14: (Color online) The mixing angle ($\theta = 0, 2\pi/8, 5\pi/8, 7\pi/8$) dependence of the effective mass plots for singlet, octet, and σ meson cases. For $\theta = 0$ in the octet case, we show only the lower bound of the Borel window since the spectral condition is not satisfied in the region $E_{th} = 0.8 \sim 1.4$ GeV.

In addition to these, we put one remark on the chiral representation of the interpolating fields: in the case of $J(\pi/4)$, i.e., the combination of $[(\mathbf{8}, \mathbf{1}) \otimes (\mathbf{1}, \mathbf{8})]$ and $(\mathbf{1}, \bar{\mathbf{1}})$ representations, the contributions from annihilation diagrams vanish (see also OPE expression), and the results of singlet, octet, and σ meson degenerate.

Taking into account the above all remarks, we evaluate the mass for singlet, octet, and σ meson cases. We mainly consider the cases of $\theta = 0$ and $7\pi/8$ in Fig.14.

For the singlet case, the typical effective mass ranges are from 600 MeV to 850 MeV in wide Borel windows with reasonable Borel stability. The E_{th} dependence is also reasonably small. For the octet case, we must avoid $\theta \sim 0$. The $\theta \sim 7\pi/8$ case was already discussed in Sec.IV B. Finally, for σ meson case, the behavior of effective mass plot is better than both singlet and octet cases. We evaluate the mass as 600 \sim 800 MeV.

- [1] For review, F.E. Close and N.A. Törnqvist, J. Phys. G: Nucl. Part. Phys. **28** (2002) R249.
 [2] R.L. Jaffe, Phys. Rev. D **15**, 267 (1977).
 [3] M. G. Alford and R. L. Jaffe, Nucl. Phys. **B578**, 367 (2000).

- [4] N. Mathur *et al.*, Phys. Rev. D **76**, 114505 (2007).
 [5] R.L. Jaffe, Phys. Rept. **409**, 1 (2005); Nucl. Phys. Proc. Suppl. **142**, 343 (2005); R.L. Jaffe and F. Wilczek, Phys. Rev. Lett. **91**, 232003 (2003).
 [6] D. Baillin and A. Love, Phys. Rep. **107**, 325 (1984); M.

Effective residue plot

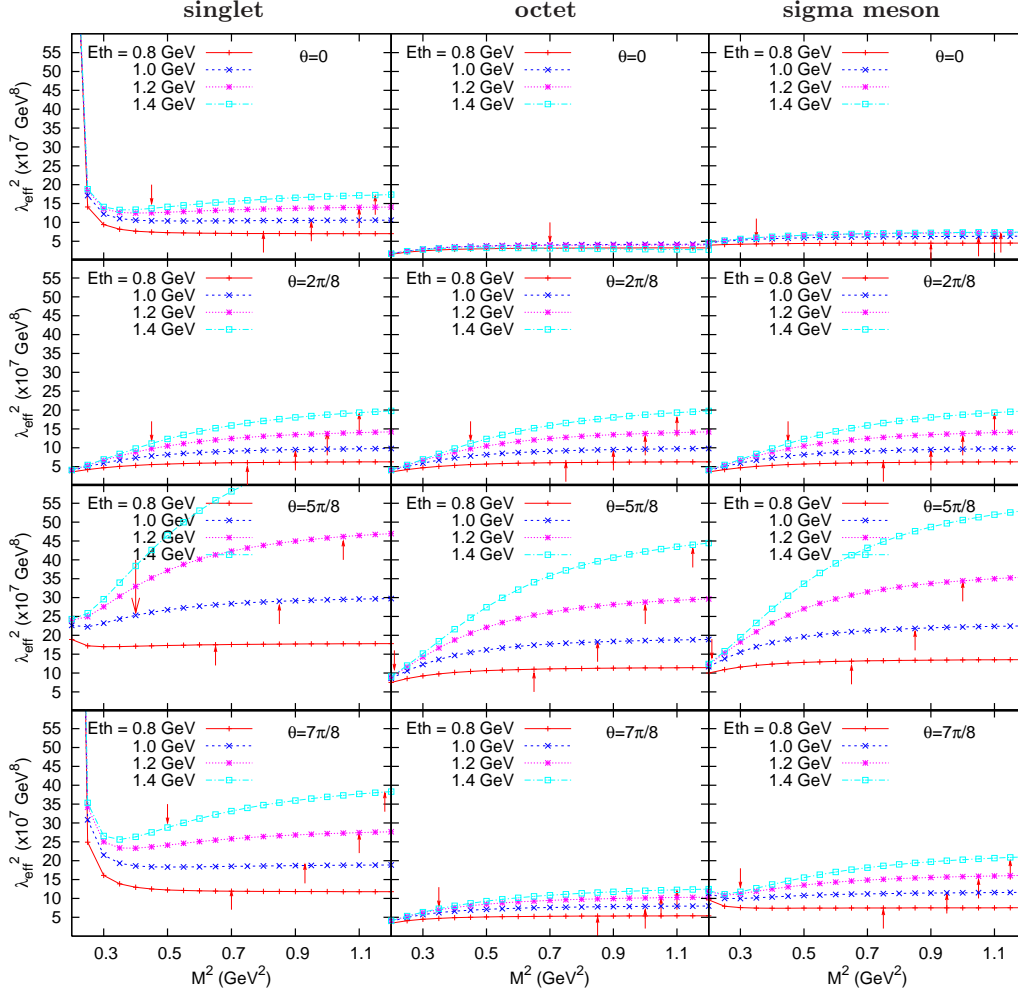


FIG. 15: (Color online) The mixing angle ($\theta = 0, 2\pi/8, 5\pi/8, 7\pi/8$) dependence of the effective residue plots for singlet, octet, and σ meson cases. For $\theta = 0$ in the octet case, we show only the lower bound of the Borel window since the spectral condition is not satisfied in the region $E_{th} = 0.8 \sim 1.4$ GeV.

- Alford, K. Rajagopal, and F. Wilczek, Phys. Lett. B **422**, 247 (1998); K. Nawa, E. Nakano, and H. Yabu, Phys. Rev. D **74**, 034017 (2006).
- [7] D. Black, A.H. Fariborz, and J. Schechter, Phys. Rev. D **69**, 035201 (2001); A.H. Fariborz, R. Jora and J. Schechter, Phys. Rev. D **72**, 034001 (2005); N. A. Törnqvist, hep-ph/0201171; hep-ph/0204215.
- [8] S. Narison, Phys. Rev. D **73**, 114024 (2006).
- [9] M.A. Shifman, A.I. Vainshtein and V.I. Zakharov, Nucl. Phys. **B147**, 385 (1979).
- [10] L.J. Reinders, H. Rubinstein and S. Yazaki, Phys. Rep. **127**, 1(1985).
- [11] S. Narison, Lecture Notes in Physics Vol. 26 (World Scientific, Singapore, 1989)
- [12] G.S. Bali *et al.* (UKQCD), Phys. Lett. B **309**, 378 (1993); C.J. Morningstar and M.J. Peardon, Phys. Rev. D **56**, 4043 (1997); Y. Chen *et al.*, Phys. Rev. D **73**, 014516 (2006).
- [13] W. Lee and D. Weingarten, Phys. Rev. D **61**, 014015 (1999); A. Hart *et al.*, Phys. Rev. D **74**, 114504 (2006); For an indirect evidence from full QCD calculation for the disconnected diagrams, T. Kunihiro *et al.*, (Scalar Collaboration), Phys. Rev. D **70**, 034504 (2004).
- [14] J. A. Oller, E. Oset, and J. R. Pelaez, Phys. Rev. D **59**, 074001 (1999); J. A. Oller and E. Oset, Nucl. Phys. **A620**, 438 (1997); Phys. Rev. D **60**, 074023 (1999); K. Igi and K. Hikasa, Phys. Rev. **D59**, 034005 (1999).
- [15] M.H. Johnson and E. Teller, Phys. Rev. **98**, 783 (1955).
- [16] For example, T. Hatsuda and T. Kunihiro, Phys. Rep. **247**, 221 (1994).
- [17] Fermilab E791 Collaboration, E.M. Aitala *et al.*, Phys. Rev. Lett. **86**, 770 (2001).
- [18] BES Collaboration, M. Ablikim *et al.*, Phys. Lett. B **598**, 149 (2004).
- [19] I. Caprini, G. Colangelo and H. Leutwyler, Phys. Rev. Lett. **96**, 132001 (2006).
- [20] T. Kojo, A. Hayashigaki, and D. Jido, Phys. Rev. C **74**, 045206 (2006); T. Kojo, D. Jido, and A. Hayashigaki,

- Prog. Theor. Phys. Suppl. **168**, 58(2007). R.D. Matheus and S. Narison, Nucl. Phys. Proc. Suppl. **152**, 236 (2006).
- [21] T.V. Brito, F.S. Navarra, M. Nielsen, and M.E. Bracco, Phys. Lett. B **608**, 69 (2005).
- [22] H. X. Chen, A. Hosaka and S. L. Zhu, Phys. Lett. B **650**, 369 (2007); Phys. Rev. D **76**, 094025 (2007).
- [23] 't Hooft, Nucl. Phys. **B72**, 461 (1974); E. Witten, Nucl. Phys. **B160**, 57 (1979).
- [24] For $a_0(980)$ meson, similar conclusion is derived with explicit use of the mixing of 4q and 2q correlators in QSR including dim.12 terms, J. Sugiyama *et al.*, Phys. Rev. D **76**, 114010 (2007).
- [25] J. Weinstein and N. Isgur, Phys. Rev. Lett. **48**, 659 (1982).
- [26] T. Barnes, Phys. Lett. B **165**, 434 (1985).
- [27] T. Kojo and D. Jido, in preparation.
- [28] Here the OPE is calculated up to dim.6 and the violation of the condensate factorization is considered with factor 2. The values of the condensates is the same as those used in our analyses in this paper, summarized in Sec.IV.